

Impact of delayed acceleration feedback on the reduced classical car-following model

Gopal Krishna Kamath, Krishna Jagannathan and Gaurav Raina

Department of Electrical Engineering, Indian Institute of Technology Madras, Chennai 600 036, India

Email: {ee12d033, krishnaj, gaurav}@ee.iitm.ac.in

Abstract—Time delays play an important role in determining the qualitative dynamical properties of a platoon of self-driven vehicles driving on a straight road. In this paper, we investigate the impact of Delayed Acceleration Feedback (DAF) on the dynamics of the Reduced Classical Car-Following Model (RCCFM). We first derive the Reduced Classical Car-Following Model with Delayed Acceleration Feedback (RCCFM-DAF). Next, we demonstrate that the transition of traffic flow from the locally stable to the unstable regime occurs via a Hopf bifurcation. The analysis also yields the necessary and sufficient condition for local stability. We characterise the type of Hopf bifurcation and the asymptotic orbital stability of the emergent limit cycles for the RCCFM by using Poincaré normal forms and the center manifold theory. We then use this analysis to obtain insights into the RCCFM-DAF by means of an appropriately defined linear transformation. The analysis is complemented with a stability chart and a bifurcation diagram. Our work reveals three effects of DAF on the RCCFM: (i) Reduction in the stable region, (ii) increase in the frequency of the emergent limit cycles, and (iii) decrease in the amplitude of the emergent limit cycles. This, in turn, has two immediate repercussions: (i) Decrease in robustness to the reaction delay, and (ii) an increase in the risk of a collision due to jerky vehicular motion.

I. INTRODUCTION

In this paper, we investigate the impact of Delayed Acceleration Feedback (DAF) on the qualitative dynamical properties of a platoon of self-driven vehicles traversing a straight road. Specifically, we analyse the effects of DAF on a recently-proposed car-following model; namely, the Reduced Classical Car-Following Model (RCCFM) [6].

Delays including reaction delays, feedback delays and communication delays are known to have a variety of effects on the properties of a dynamical system [11]. For instance, they can readily lead to instability and oscillations [18], [21]. In contrast, introducing appropriately chosen delayed feedback signals are known to stabilise systems [10], [19].

In the context of car-following models (a specific class of dynamical systems), reaction delays are mostly known to have a detrimental effect. Specifically, traffic flows that result from the underlying car-following models have been shown to transit into an unstable regime with an increase in the reaction delay [6], [7]. The occurrence of a peculiar phenomenon known as a ‘phantom jam’ [2], [4] – the emergence of back-propagating congestion waves in motorway traffic, seemingly out of nowhere – has also been attributed to variations in the reaction delay [6]. In contrast, Ge *et al.* [10] showed that using appropriate DAF signals with a certain car-following

model could improve the robustness of the resulting traffic flow to reaction and communication delays. Motivated by this, in this paper, we focus on the impact of DAF on the RCCFM.

A. Related work on car-following models and DAF

Car-following models constitute a class of dynamical models for transportation networks that capture the variation in acceleration of each vehicle in a platoon. Two of the earliest works investigating the stability of car-following models are by Chandler *et al.* [14] and Herman *et al.* [16]. We base our work on the Classical Car-Following Model (CCFM) proposed in the pioneering work by Gazis *et al.* [3]. Some related models have been studied in [3], [5], and [14], and [15] is a recent exposition of linear stability analysis as applied to car-following models.

In the above works, stability conditions are derived predominantly using transform techniques. In contrast, [21] and some of the references therein consider the issue of stability from a dynamical systems perspective. Additionally, Kamath *et al.* [6] proved that the RCCFM loses stability via a Hopf bifurcation. This leads to the emergence of limit cycles (isolated closed orbits in phase space), which manifest as back-propagating congestion waves in motorway traffic.

Use of acceleration and DAF signals in feedback loops has been studied for over two decades, in various applications [8], [19], [20]. In the context of human postural balance, Insperger *et al.* [19] proposed a DAF-based Proportional Derivative Acceleration (PDA) controller and established its superiority over the classical proportional derivative controller via numerical computations. Motivated by this, Ge *et al.* [10] proposed a possible method of implementing a variant of the said PDA controller, in the context of a platoon of human-driven vehicles. This was achieved using selectively-placed connected cruise control vehicles running the Optimal Velocity Model (OVM) [12]. It was then numerically shown that appropriate usage of feedback signals could increase robustness to reaction and communication delays.

B. Our contributions

Our contributions can be summarised as follows:

1. We analytically prove that the RCCFM-DAF – a model we derive by incorporating DAF in the RCCFM – also undergoes a Hopf bifurcation. This shows that DAF preserves the mechanics by which the RCCFM loses stability. The

analysis also yields the necessary and sufficient condition for local stability of the RCCFM-DAF.

2. We deduce two detrimental effects of DAF on the RCCFM: (i) Reduction in the stable region, and (ii) increase in the frequency of the emergent limit cycles.

3. We propose a simple linear transformation by exploiting the structure of the RCCFM-DAF. This allows us to deduce the type of Hopf bifurcation and the asymptotic orbital stability of the emergent limit cycles of the RCCFM-DAF by analysing the RCCFM. This is of significance since the RCCFM-DAF is governed by a system of neutral functional differential equations, whereas the RCCFM is governed by a system of retarded functional differential equations, which are relatively easier to analyse.

4. Finally, by means of a numerically constructed bifurcation diagram, we show that the amplitude of limit cycles decreases with an increase in the DAF signal strength.

From these contributions, we conclude that DAF is detrimental to the RCCFM since it: (i) decreases the robustness to the reaction delay, and (ii) may lead to jerky vehicular motion, thereby increasing the risk of a collision.

The remainder of this paper is organised as follows. In Section II, we present the existing models relevant to our work, and derive the RCCFM-DAF. In Section III, we perform a detailed Hopf bifurcation analysis of the RCCFM-DAF. Section IV presents a numerically constructed bifurcation diagram, and we conclude in Section V.

II. MODELS

In this section, we first provide an overview of the scenario we consider. We then briefly describe two relevant models – the CCFM and the RCCFM. We end the section by deriving the RCCFM-DAF – the model we investigate in this paper.

A. The setting

We consider a platoon of $N + 1$ zero-length vehicles travelling on an infinitely long, single-lane road without overtaking. The lead vehicle is indexed 0, its follower 1, and so forth. Each vehicle updates its acceleration based on a combination of its position, velocity and acceleration and those of the vehicle directly ahead. We denote the position, velocity and acceleration of the i^{th} vehicle at time t by $x_i(t)$, $\dot{x}_i(t)$ and $\ddot{x}_i(t)$ respectively. The acceleration and velocity profiles of the lead vehicle are assumed to be known. In particular, we restrict ourselves to leader profiles that converge, in finite time, to $\ddot{x}_0 = 0$ and $\dot{x}_0 < \infty$; that is, there exists a finite T_0 such that $\ddot{x}_0(t) = 0$, $\dot{x}_0(t) = \dot{x}_0$, $\forall t \geq T_0$. We use the terms “driver” and “vehicle” interchangeably.

B. The Classical Car-Following Model (CCFM)

The acceleration of each vehicle running the CCFM is updated depending on: (i) its own velocity, (ii) the velocity relative to the vehicle directly ahead, and (iii) distance to the vehicle directly ahead [3]. Symbolically,

$$\ddot{x}_i(t) = \alpha_i \frac{(\dot{x}_i(t))^m (\dot{x}_{i-1}(t - \tau) - \dot{x}_i(t - \tau))}{(x_{i-1}(t - \tau) - x_i(t - \tau))^l}, \quad (1)$$

for $i \in \{1, 2, \dots, N\}$. Here, $\alpha_i > 0$ represents the i^{th} driver’s sensitivity coefficient. Also, $m \in [-2, 2]$ and $l \in \mathbb{R}_+$ are model parameters that contribute to the non-linearity.

Following [21], we set $y_i(t) + b = x_{i-1}(t) - x_i(t)$ and $v_i(t) = \dot{y}_i(t) = \dot{x}_{i-1}(t) - \dot{x}_i(t)$. Thus, system (1) becomes:

$$\begin{aligned} \dot{v}_i(t) &= \beta_{i-1}(t)v_{i-1}(t - \tau) - \beta_i(t)v_i(t - \tau), \\ \dot{y}_i(t) &= v_i(t), \end{aligned} \quad (2)$$

for $i \in \{1, 2, \dots, N\}$. Here,

$$\beta_i(t) = \alpha_i \frac{(\dot{x}_0(t) - v_0(t) - \dots - v_i(t))^m}{(y_i(t - \tau) + b)^l}.$$

Here, b denotes the desired equilibrium separation, $y_i(t) + b$ represents the separation between vehicles $i - 1$ and i at time t , and $v_i(t)$ corresponds to the relative velocity of the i^{th} vehicle with respect to the $(i - 1)^{\text{th}}$ vehicle at time t . Note that y_0 , v_0 , α_0 and τ_0 are dummy variables introduced for notational brevity, all of which are set to zero. We emphasise that y_0 and v_0 are *not* state variables.

C. The Reduced Classical Car-Following Model (RCCFM)

The RCCFM was obtained in [6] by setting $l = 0$ in the CCFM. This restriction decouples the dynamics of v_i from that of y_i for each i . Hence, the state variables $\{y_i\}_{i=1}^N$ in (2) are dropped, resulting in the RCCFM, described by

$$\dot{v}_i(t) = \beta_{i-1}(t - \tau_{i-1})v_{i-1}(t - \tau_{i-1}) - \beta_i(t - \tau_i)v_i(t - \tau_i), \quad (3)$$

for $i \in \{1, 2, \dots, N\}$. Since $l = 0$, $\beta_i(t)$ is now given by $\alpha_i (\dot{x}_0(t) - v_0(t) - \dots - v_i(t))^m$.

Observe the generalizations incorporated in the RCCFM: (i) The self-velocity term, captured by $\beta_i(t)$, is delayed, and (ii) heterogeneity in reaction delays has been accounted for.

D. The Reduced Classical Car-Following Model with Delayed Acceleration Feedback (RCCFM-DAF)

We now derive the RCCFM-DAF, to be analysed in the next section. We begin with (1) when $l = 0$, albeit with a delayed self-velocity term, as suggested in [6]. That is,

$$\ddot{x}_i(t) = \alpha_i (\dot{x}_i(t - \tau))^m (\dot{x}_{i-1}(t - \tau) - \dot{x}_i(t - \tau)), \quad (4)$$

for $i \in \{1, 2, \dots, N\}$. Following [19], we introduce a delayed acceleration term in the above equation to obtain

$$\ddot{x}_i(t) = \alpha_i (\dot{x}_i(t - \tau))^m (\dot{x}_{i-1}(t - \tau) - \dot{x}_i(t - \tau)) + \gamma \ddot{x}_i(t - \tau), \quad (5)$$

for $i \in \{1, 2, \dots, N\}$. Here, $\gamma > 0$ captures the sensitivity towards delayed acceleration. Transforming (5) similar to the RCCFM, accounting for the heterogeneity in reaction delays and sensitivity coefficients, and re-arranging the terms, we obtain the following system:

$$\begin{aligned} \dot{v}_1(t) - \gamma_1 \dot{v}_1(t - \tau_1) &= \ddot{x}_0(t) - \gamma_1 \ddot{x}_0(t - \tau_1) \\ &\quad - \beta_1(t - \tau_1)v_1(t - \tau_1), \\ \dot{v}_k(t) - \gamma_k \dot{v}_k(t - \tau_k) &= \beta_{k-1}(t - \tau_{k-1})v_{k-1}(t - \tau_{k-1}) \\ &\quad - \beta_k(t - \tau_k)v_k(t - \tau_k), \end{aligned} \quad (6)$$

for $k \in \{2, 3, \dots, N\}$ and $\beta_i(t)$ as in the RCCFM. We refer to system (6) as the Reduced Classical Car-Following

Model with Delayed Acceleration Feedback (RCCFM-DAF). We note that system (6) is a system of neutral functional differential equation [11, Section 2.7], since the highest order derivative of the state variable is delayed. We also note that the delay incurred while sensing the acceleration signal is negligible. However, to analyse the RCCFM-DAF in a general setting, no approximations are used.

III. THE HOPF BIFURCATION

Hopf bifurcation [1] is a phenomenon wherein a dynamical system undergoes a stability switch due to a pair of conjugate eigenvalues crossing the imaginary axis in the Argand plane. Mathematically, a Hopf bifurcation analysis is a rigorous way of proving the emergence of limit cycles in non-linear dynamical systems.

In this section, we first linearise the RCCFM-DAF described by (6) and prove the transversality condition of the Hopf spectrum [11, Chapter 11, Theorem 1.1] using reaction delay as the ‘bifurcation parameter.’ This shows that the RCCFM-DAF loses local stability via a Hopf bifurcation. The analysis also yields the necessary and sufficient condition for local stability. We then perform a detailed local bifurcation analysis of the RCCFM to determine the type of Hopf bifurcation and the asymptotic orbital stability of the resulting limit cycle. We use an appropriately chosen linear transformation to obtain insights into the RCCFM-DAF.

A. Transversality condition of the Hopf spectrum

It is clear that $v_i^* = 0$, $i = 1, 2, \dots, N$ is an equilibrium for system (6). Linearising system (6) about this equilibrium, and setting the leader’s profile to zero, we obtain

$$\dot{v}_i(t) = \beta_{i-1}^* v_{i-1}(t - \tau_{i-1}) - \beta_i^* v_i(t - \tau_i) + \gamma_i \dot{v}_i(t - \tau_i), \quad (7)$$

for $i \in \{1, 2, \dots, N\}$. Here, $\beta_i^* = \alpha_i (\dot{x}_0)^m$ denotes the equilibrium coefficient for the i^{th} vehicle. System (7) can be succinctly written using matrix representation as

$$\dot{s}(t) = \sum_{k=1}^N (A_k s(t - \tau_k) + B_k \dot{s}(t - \tau_k)), \quad (8)$$

where $s(t) = [v_1(t) v_2(t) \dots v_N(t)]^T$ and $A_k, B_k \in \mathbb{R}^{N \times N} \forall k$. In fact, for $k \in \{1, 2, \dots, N\}$,

$$(B_k)_{ij} = \begin{cases} \gamma_k, & i = j = k, \\ 0, & \text{otherwise.} \end{cases}$$

Also, for $k \in \{1, 2, \dots, N - 1\}$,

$$(A_k)_{ij} = \begin{cases} -\beta_k^*, & i = j = k, \\ \beta_k^*, & j = k, i = k + 1, \\ 0, & \text{otherwise,} \end{cases}$$

and

$$(A_N)_{ij} = \begin{cases} -\beta_N^*, & i = j = k, \\ 0, & \text{otherwise.} \end{cases}$$

The characteristic equation pertaining to systems of the form (8), derived by generalising the calculations given in [9, Section 5.1], is given by

$$f(\lambda) = \det \left(\lambda I_{N \times N} - \sum_{k=1}^N (e^{-\lambda \tau_k} A_k + \lambda e^{-\lambda \tau_k} B_k) \right) = 0,$$

which then simplifies to

$$f(\lambda) = \prod_{i=1}^N (\lambda - \gamma_i \lambda e^{-\lambda \tau_i} + \beta_i^* e^{-\lambda \tau_i}) = 0. \quad (9)$$

We consider the case when exactly one term in (9) is zero as this corresponds to the typical system behaviour. Therefore, for some $i \in \{1, 2, \dots, N\}$, we have:

$$\lambda - \gamma_i \lambda e^{-\lambda \tau_i} + \beta_i^* e^{-\lambda \tau_i} = 0. \quad (10)$$

Since (6) is of neutral type, for system stability to be characterised by the roots of (10) lying in the open left half of the Argand plane, $\gamma_i < 1$ must be satisfied [11, Section 1.7]. Hence, we enforce this constraint and search for a conjugate pair of eigenvalues of (10) that crosses the imaginary axis in the Argand plane, thereby pushing the system into an unstable regime. To that end, we substitute $\lambda = j\omega$, with $j = \sqrt{-1}$, in (10) to obtain

$$\begin{aligned} \beta_i^* \cos(\omega \tau_i) - \gamma_i \omega \sin(\omega \tau_i) &= 0, \\ \omega - \gamma_i \omega \cos(\omega \tau_i) - \beta_i^* \sin(\omega \tau_i) &= 0. \end{aligned}$$

The first equality implies $\beta_i^* = \gamma_i \omega \tan(\omega \tau_i)$. Substituting for β_i^* in the second equality and simplifying yields $\cos(\omega \tau_i) = \gamma_i$ and $\sin(\omega \tau_i) = \beta_i^* / \omega$. Squaring, adding and simplifying, we obtain the angular velocity of the oscillations as

$$\omega_0 = \frac{\beta_i^*}{\sqrt{1 - \gamma_i^2}}.$$

We note that $\omega_0 > 0$ since $\gamma_i < 1$. Therefore, when a conjugate pair of eigenvalues is on the imaginary axis in the Argand plane, we have:

$$\omega_0 = \frac{\beta_i^*}{\sqrt{1 - \gamma_i^2}}, \quad (11)$$

$$\tau_{i_{cr}} = \frac{1}{\omega_0} \tan^{-1} \left(\frac{\beta_i^*}{\gamma_i \omega_0} \right), \quad (12)$$

where $\tau_{i_{cr}}$ is the critical value of the delay when $\omega = \omega_0$.

To show that system (6) undergoes a Hopf bifurcation at $\tau_i = \tau_{i_{cr}}$, we need to prove the transversality condition of the Hopf spectrum [11, Chapter 11, Theorem 1.1]:

$$\text{Real} \left(\frac{d\lambda}{d\tau_i} \right)_{\tau_i = \tau_{i_{cr}}} \neq 0. \quad (13)$$

Therefore, we differentiate (10) with respect to τ_i . Upon manipulating the resulting equations and simplifying, we obtain

$$\text{Real} \left(\frac{d\lambda}{d\tau_i} \right)_{\tau_i = \tau_{i_{cr}}} = \frac{\omega_0^2 (1 - \gamma_i^2)}{\tilde{\theta}} > 0, \quad (14)$$

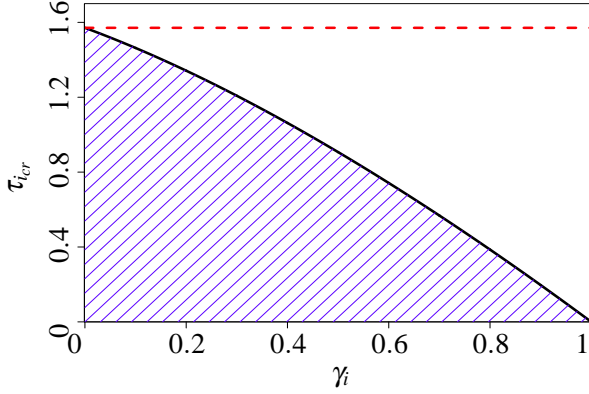


Fig. 1. For any RCCFM-DAF system with $\beta_i^* = 1$, the shaded portion represents the stable region. Black solid line portrays the decreasing trend of the left hand side of (17) with respect to γ_i . Red dashed line indicates $\pi/2$, for reference.

where $\tilde{\theta} = (1 - \gamma_i \cos(\omega_0 \tau_i))^2 + (\omega_0 \tau_i + \gamma_i \sin(\omega_0 \tau_i))^2$. Also note that the positivity of the Right Hand Side (RHS) is a consequence of the imposed condition $\gamma_i < 1$.

The above result implies that system (6) undergoes a Hopf bifurcation at $\tau_i = \tau_{i,cr}$. Hence, $\tau_i < \tau_{i,cr}$ is the necessary and sufficient condition for system (6) to be locally stable when the neutral condition $\gamma_i < 1$ is satisfied. This, in turn, implies that if $\gamma_i < 1$, then $\tau_i = \tau_{i,cr}$ is the equation of the stability boundary, also known as the Hopf boundary.

To understand the effect of DAF, we compare the critical values of the reaction delay under the RCCFM-DAF and the RCCFM. To that end, we first simplify (12), to obtain

$$\tau_{i,cr} = \frac{\sqrt{1 - \gamma_i^2}}{\beta_i^*} \tan^{-1} \left(\frac{\sqrt{1 - \gamma_i^2}}{\gamma_i} \right). \quad (15)$$

The critical value of the reaction delay under the RCCFM, denoted by $\tilde{\tau}_{i,cr}$, can shown to be [6]

$$\tilde{\tau}_{i,cr} = \frac{\pi}{2\beta_i^*}. \quad (16)$$

To compare (15) and (16), it suffices to find a γ_i such that

$$\sqrt{1 - \gamma_i^2} \tan^{-1} \left(\frac{\sqrt{1 - \gamma_i^2}}{\gamma_i} \right) \geq \frac{\pi}{2}, \quad (17)$$

holds. This is desired since it would ensure a larger (in the sense of set containment) stable region. Note that (17) is trivially met with equality for $\gamma_i = 0$, whence system (6) collapses to system (3). Fig. 1 shows the variation of the left hand side of (17) with respect to γ_i . Clearly, there does not exist a non-trivial γ_i satisfying (17). This implies that DAF is detrimental to the stability of the RCCFM. In fact, Fig. 1 represents the stability chart for systems with $\beta_i^* = 1$. We see that the range of reaction delays that stabilises the system decreases rapidly with an increase in γ_i .

A few remarks are in order. First, we note that the system loses stability when the very first conjugate pair of

eigenvalues crosses the imaginary axis. Further increase in τ_i cannot restore system stability – indeed, the derivative in (14) is positive. That is, an increase in τ_i results in the eigenvalues moving to the right in the Argand plane, making it impossible to regain lost stability. Next, we note that the value of $\tau_{i,cr}$ depends on other system parameters as well. Hence, an appropriate variation in *any* of these parameters could lead to loss of system stability. Thus, any of these parameters can be used as the bifurcation parameter. Further, observe that $f_0 = \omega_0/2\pi$, obtained from (11), represents the frequency of the emergent oscillations. From [6], the frequency of oscillations under the RCCFM is given by $\tilde{f}_0 = \beta_i^*/2\pi$. We note that $f_0 \geq \tilde{f}_0$. That is, in addition to shrinking the stable region, DAF also leads to oscillations of a higher frequency. Lastly, we note that an expression similar to (16) was derived in [17], albeit in a different context. Hence, our results apply to any system similar to system (3), and not just the RCCFM.

B. Hopf bifurcation analysis

Having proved the transversality condition of the Hopf spectrum, we now characterise the *type* of Hopf bifurcation and the asymptotic *orbital stability* of the resulting limit cycles, following the style of analysis presented in [1].

For ease of exposition, we begin by denoting $v_i(t) - \gamma_i v_i(t - \tau_i)$ by $l_i(t)$ in (6). Therefore, the RHS of (6) captures the dynamics of $l_i(t)$. That is, for $i \in \{1, 2, \dots, N\}$,

$$\dot{l}_i(t) = \beta_{i-1}(t - \tau_{i-1}) v_{i-1}(t - \tau_{i-1}) - \beta_i(t - \tau_i) v_i(t - \tau_i). \quad (18)$$

Note that $l_i(t) = \langle c, \mathbf{v}(t) \rangle = [1 - \gamma_i][v_i(t) v_i(t - \tau_i)]^T$, where $c = [1 - \gamma_i]^T$ and $\mathbf{v}(t) = [v_i(t) v_i(t - \tau_i)]^T$. We now prove a result, which we then use for our specific system.

Lemma 1: Let $x(t) = [x_1(t) x_2(t)]^T$ and $c = [c_1 c_2]^T$, where x_1 and x_2 are bounded, non-constant real-valued functions and c_1 and c_2 are non-zero, real constants. Also, let $y(t) = \langle c, x(t) \rangle = c_1 x_1(t) + c_2 x_2(t)$. Then, $y(t)$ is periodic if and only if $x(t)$ is periodic. Moreover, $x(t)$ and $y(t)$ will have the same period.

Proof: First, let $x(t)$ be periodic with period $T > 0$, *i.e.*, $x(t + T) = x(t) \forall t$. Then, $y(t + T) = \langle c, x(t + T) \rangle = \langle c, x(t) \rangle = y(t) \forall t$. Hence, $y(t)$ is periodic with period T . Conversely, assume that $y(t)$ is periodic with period $T > 0$, *i.e.*, $y(t + T) = y(t) \forall t$. Then, $\langle c, x(t + T) \rangle = \langle c, x(t) \rangle \forall t$. Therefore, $\langle c, x(t) - x(t + T) \rangle = 0 \forall t$. Since c_1 and c_2 are non-zero, the assumptions on x_1 and x_2 imply that $x(t) = x(t + T)$, *i.e.*, $x(t)$ is periodic with period T . \square

In the context of the RCCFM-DAF, Lemma 1 implies that $v_i(t)$ is periodic if and only if $l_i(t)$ is periodic, and that their periods coincide. Moreover, this equivalence also implies that the aforementioned transformation preserves the topological changes in the phase space, *i.e.*, $v_i(t)$ would undergo the same type of Hopf bifurcation as $l_i(t)$ and the emergent limit cycles would have the same asymptotic orbital stability. Therefore, we now characterise the type of Hopf bifurcation that $l_i(t)$ undergoes, and the asymptotic orbital stability of the emergent limit cycles.

We begin by denoting $\mu = \tau_i - \tau_{i_{cr}}$. Observe that the system undergoes a Hopf bifurcation at $\mu = 0$, where $\tau_i = \tau_{i_{cr}}$. Henceforth, we consider μ as the bifurcation parameter. An incremental change in τ_i from $\tau_{i_{cr}}$ to $\tau_{i_{cr}} + \mu$, where $\mu > 0$, pushes the system in to its unstable regime. We now provide a concise step-by-step overview of the detailed local bifurcation analysis, before delving into the technical details.

Step 1: Using the Taylor series expansion, we segregate the RHS of (18) into linear and non-linear parts. We then cast this into the standard form of an Operator Differential Equation (OpDE).

Step 2: At the critical value of the bifurcation parameter, *i.e.*, at $\mu = 0$, the system has exactly one pair of purely imaginary eigenvalues with non-zero angular velocity, as given by (11). The linear eigenspace spanned by the corresponding eigenvectors is called the critical eigenspace. The center manifold theorem [1] guarantees the existence of a locally invariant 2-dimensional manifold that is tangent to the critical eigenspace at the equilibrium of the system.

Step 3: Next, we project the system onto its critical eigenspace as well as its complement, at the critical value of the bifurcation parameter. This helps describe the dynamics of the system on the center manifold, with the aid of an ordinary differential equation in a single complex variable.

Step 4: Finally, using Poincaré normal forms, we evaluate the Lyapunov coefficient and the Floquet exponent, which characterise the type of the Hopf bifurcation and the asymptotic orbital stability of the emergent limit cycles respectively.

We begin the analysis by expanding (18) about the all-zero equilibrium using Taylor's series, to obtain

$$\begin{aligned} \dot{l}_i(t) = & -\beta_i^* v_{i,t}(-\tau_i) + \beta_{i-1}^* v_{(i-1),t}(-\tau_{i-1}) \\ & + \left(\frac{2m\beta_i^*}{\dot{x}_0} \right) \sum_{l=1}^i v_{l,t}(-\tau_i) v_{i,t}(-\tau_i) \\ & - \left(\frac{2m\beta_{i-1}^*}{\dot{x}_0} \right) \sum_{l=1}^{i-1} v_{l,t}(-\tau_{i-1}) v_{(i-1),t}(-\tau_{i-1}) \\ & - \left(\frac{12m(m-1)\beta_i^*}{\dot{x}_0^2} \right) \sum_{n=1}^i \sum_{l=1}^i v_{l,t}(-\tau_i) v_{n,t}(-\tau_i) v_{i,t}(-\tau_i) \\ & + \left(\frac{12m(m-1)\beta_{i-1}^*}{\dot{x}_0^2} \right) \times \\ & \sum_{n=1}^{i-1} \sum_{l=1}^{i-1} v_{l,t}(-\tau_{i-1}) v_{n,t}(-\tau_{i-1}) v_{(i-1),t}(-\tau_{i-1}) \\ & + \text{higher order terms,} \end{aligned} \quad (19)$$

where $v_{i,t}(\theta) \triangleq v_i(t+\theta)$. In the following, we use $\mathcal{C}^k(A; B)$ to denote the linear space of all functions from A to B which are k times differentiable, with each derivative being continuous. Also, we use \mathcal{C} to denote \mathcal{C}^0 , for convenience.

We define $\mathbf{L}(t) \triangleq [l_1(t) \ l_2(t) \ \cdots \ l_N(t)]^T$, and note that (6) is of the form:

$$\frac{d\mathbf{L}(t)}{dt} = \mathcal{L}_\mu \mathbf{L}_t(\theta) + \mathcal{F}(\mathbf{L}_t(\theta), \mu), \quad (20)$$

where $t > 0$, $\mu \in \mathbb{R}$, and where for $\tau = \max_i \tau_i > 0$,

$$\mathbf{L}_t(\theta) = \mathbf{L}(t+\theta), \quad \mathbf{L} : [-\tau, 0] \longrightarrow \mathbb{R}^N, \quad \theta \in [-\tau, 0].$$

Here, $\mathcal{L}_\mu : \mathcal{C}([-\tau, 0]; \mathbb{R}^N) \longrightarrow \mathbb{R}^N$ is a one-parameter family of continuous, bounded linear functionals, whereas the operator $\mathcal{F} : \mathcal{C}([-\tau, 0]; \mathbb{R}^N) \longrightarrow \mathbb{R}^N$ is an aggregation of the non-linear terms. Further, we assume that $\mathcal{F}(\mathbf{L}_t, \mu)$ is analytic, and that \mathcal{F} and \mathcal{L}_μ depend analytically on the bifurcation parameter μ , for small $|\mu|$. The objective now is to cast (20) in the standard form of an OpDE:

$$\frac{d\mathbf{L}_t}{dt} = \mathcal{A}(\mu)\mathbf{L}_t + \mathcal{R}\mathbf{L}_t, \quad (21)$$

since the dependence here is on \mathbf{L}_t alone rather than both \mathbf{L}_t and $\mathbf{L}(t)$. To that end, we begin by transforming the linear problem $d\mathbf{L}(t)/dt = \mathcal{L}_\mu \mathbf{L}_t(\theta)$. We note that, by the *Riesz representation theorem* [22, Theorem 6.19], there exists an $N \times N$ matrix-valued measure $\eta(\cdot, \mu) : \mathcal{B}(\mathcal{C}([-\tau, 0]; \mathbb{R}^N)) \longrightarrow \mathbb{R}^{N \times N}$, wherein each component of $\eta(\cdot)$ has bounded variation, and for all $\phi \in \mathcal{C}([-\tau, 0]; \mathbb{R}^N)$, we have

$$\mathcal{L}_\mu \phi = \int_{-\tau}^0 d\eta(\theta, \mu) \phi(\theta). \quad (22)$$

In particular,

$$\mathcal{L}_\mu \mathbf{L}_t = \int_{-\tau}^0 d\eta(\theta, \mu) \mathbf{L}(t+\theta).$$

Motivated by the linearised system (7), we define

$$(\mathrm{d}\eta)_{ij} = \begin{cases} -\beta_i^* \delta(\theta + \tau_i), & i = j, \\ \beta_j^* \delta(\theta + \tau_j), & j = i - 1, i > 1, \\ 0, & \text{otherwise,} \end{cases}$$

where $\delta(\cdot)$ denotes the Dirac delta. Observe that $d\eta = (\mathrm{d}\eta)_{i,j=1}^N d\theta$ as defined above satisfies (22).

For $\phi \in \mathcal{C}^1([-\tau, 0]; \mathbb{C}^N)$, we define

$$\mathcal{A}(\mu)\phi(\theta) = \begin{cases} \frac{d\phi(\theta)}{d\theta}, & \theta \in [-\tau, 0), \\ \int_{-\tau}^0 d\eta(s, \mu) \phi(s) \equiv \mathcal{L}_\mu, & \theta = 0, \end{cases} \quad (23)$$

and

$$\mathcal{R}\phi(\theta) = \begin{cases} 0, & \theta \in [-\tau, 0), \\ \mathcal{F}(\phi, \mu), & \theta = 0. \end{cases}$$

With the above definitions, we observe that $d\mathbf{L}_t/d\theta \equiv d\mathbf{L}_t/dt$. Hence, we have successfully cast (20) in the form of (21). To obtain the required coefficients, it is sufficient to evaluate various expressions for $\mu = 0$, which we use henceforth. We start by finding the eigenvector of the operator $\mathcal{A}(0)$ with eigenvalue $\lambda(0) = j\omega_0$. That is, we want an $N \times 1$ vector (to be denoted by $q(\theta)$) with the property that $\mathcal{A}(0)q(\theta) = j\omega_0 q(\theta)$. We assume the form: $q(\theta) = [1 \ \phi_1 \ \phi_2 \ \cdots \ \phi_{N-1}]^T e^{j\omega_0 \theta}$, and solve the eigenvalue equation to obtain, for $i \in \{1, 2, \dots, N-1\}$,

$$\phi_i = \frac{\beta_i^* e^{-j\omega_0 \tau_i}}{j\omega_0 + \beta_{i+1}^* e^{-j\omega_0 \tau_{i+1}}} \phi_{i-1},$$

where we set $\phi_0 = 1$ for notational brevity.

We define the *adjoint* operator as follows:

$$\mathcal{A}^*(0)\phi(\theta) = \begin{cases} -\frac{d\phi(\theta)}{d\theta}, & \theta \in (0, \tau], \\ 0 & \theta = 0, \\ \int_{-\tau}^0 d\eta^T(s, 0)\phi(-s), & \theta = 0, \end{cases}$$

where $d\eta^T$ is the transpose of $d\eta$. We note that the domains of \mathcal{A} and \mathcal{A}^* are $\mathcal{C}^1([-\tau, 0]; \mathbb{C}^N)$ and $\mathcal{C}^1([0, \tau]; \mathbb{C}^N)$ respectively. Therefore, if $j\omega_0$ is an eigenvalue of \mathcal{A} , then $-j\omega_0$ is an eigenvalue of \mathcal{A}^* . Hence, to find the eigenvector of $\mathcal{A}^*(0)$ corresponding to $-j\omega_0$ (to be denoted by $p(\theta)$), we assume the form: $p(\theta) = B[\psi_{N-1} \ \psi_{N-2} \ \psi_{N-3} \ \cdots \ 1]^T e^{j\omega_0\theta}$, and solve $\mathcal{A}^*(0)p(\theta) = -j\omega_0 p(\theta)$ to obtain, for $i \in \{1, 2, \dots, N-1\}$,

$$\psi_i = \frac{\beta_{N-i}^* e^{j\omega_0\tau_{N-i}}}{\beta_{N-i}^* e^{j\omega_0\tau_{N-i}} - j\omega_0} \psi_{i-1},$$

where we set $\psi_0 = 1$ for notational brevity. Further, the normalization condition for Hopf bifurcation requires that $\langle p, q \rangle = 1$, thus yielding an expression for B .

For any $q \in \mathcal{C}([-\tau, 0]; \mathbb{C}^N)$ and $p \in \mathcal{C}([0, \tau]; \mathbb{C}^N)$, the inner product is defined as

$$\langle p, q \rangle \triangleq \bar{p} \cdot q - \int_{\theta=-\tau}^0 \int_{\zeta=0}^{\theta} \bar{p}^T(\zeta - \theta) d\eta q(\zeta) d\zeta, \quad (24)$$

where the overbar represents the complex conjugate and the “ \cdot ” represents the regular dot product. Simplifying (24) and equating to unity yields

$$\bar{B} = \frac{1}{\zeta_1 + \zeta_2}, \text{ where,}$$

$$\zeta_1 = \sum_{k=0}^{N-1} \bar{\psi}_{N-1-k} \phi_k, \text{ and}$$

$$\zeta_2 = \sum_{n=1}^N (\beta_n^* \tau_n e^{-j\omega_0\tau_n} \phi_{n-1} (\bar{\psi}_{N-n} - \bar{\psi}_{N-n-1})).$$

For \mathbf{L}_t , a solution of (21) at $\mu = 0$, we define

$$z(t) = \langle p(\theta), \mathbf{L}_t \rangle, \text{ and,}$$

$$\mathbf{w}(t, \theta) = \mathbf{L}_t(\theta) - 2\text{Real}(z(t)q(\theta)).$$

Then, on the center manifold C_0 , we have $\mathbf{w}(t, \theta) = \mathbf{w}(z(t), \bar{z}(t), \theta)$, where

$$\mathbf{w}(z(t), \bar{z}(t), \theta) = \mathbf{w}_{20}(\theta) \frac{z^2}{2} + \mathbf{w}_{02}(\theta) \frac{\bar{z}^2}{2} + \mathbf{w}_{11}(\theta) z\bar{z} + \cdots \quad (25)$$

Effectively, z and \bar{z} are the local coordinates for C_0 in \mathcal{C} in the directions of p and \bar{p} respectively. We note that \mathbf{w} is real if \mathbf{L}_t is real, and we deal only with real solutions. The existence of the center manifold C_0 enables the reduction of (21) to an Ordinary Differential Equation (ODE) in a single complex variable on C_0 . At $\mu = 0$, the said ODE can be described as

$$\begin{aligned} \dot{z}(t) &= \langle p, \mathcal{A}\mathbf{L}_t + \mathcal{R}\mathbf{L}_t \rangle, \\ &= j\omega_0 z(t) + \bar{p}(0) \cdot \mathcal{F}(\mathbf{w}(z, \bar{z}, \theta) + 2\text{Real}(z(t)q(\theta))), \\ &= j\omega_0 z(t) + \bar{p}(0) \cdot \mathcal{F}_0(z, \bar{z}). \end{aligned} \quad (26)$$

This is written in abbreviated form as

$$\dot{z}(t) = j\omega_0 z(t) + g(z, \bar{z}). \quad (27)$$

The objective now is to expand g in powers of z and \bar{z} . However, this requires $\mathbf{w}_{ij}(\theta)$'s from (25). Once these are evaluated, the ODE (26) for z would be explicit (as given by (27)), where g can be expanded in terms of z and \bar{z} as

$$\begin{aligned} g(z, \bar{z}) &= \bar{p}(0) \cdot \mathcal{F}_0(z, \bar{z}) \\ &= g_{20} \frac{z^2}{2} + g_{02} \frac{\bar{z}^2}{2} + g_{11} z\bar{z} + g_{21} \frac{z^2\bar{z}}{2} + \cdots \end{aligned} \quad (28)$$

Next, we write $\dot{\mathbf{w}} = \dot{\mathbf{L}}_t - \dot{z}q - \dot{\bar{z}}\bar{q}$. Using (21) and (27), we then obtain the following ODE:

$$\dot{\mathbf{w}} = \begin{cases} \mathcal{A}\mathbf{w} - 2\text{Real}(\bar{p}(0) \cdot \mathcal{F}_0 q(\theta)), & \theta \in [-\tau, 0), \\ \mathcal{A}\mathbf{w} - 2\text{Real}(\bar{p}(0) \cdot \mathcal{F}_0 q(0)) + \mathcal{F}_0, & \theta = 0. \end{cases}$$

This can be re-written using (25) as

$$\dot{\mathbf{w}} = \mathcal{A}\mathbf{w} + H(z, \bar{z}, \theta), \quad (29)$$

where H can be expanded as

$$\begin{aligned} H(z, \bar{z}, \theta) &= H_{20}(\theta) \frac{z^2}{2} + H_{02}(\theta) \frac{\bar{z}^2}{2} + H_{11}(\theta) z\bar{z} \\ &\quad + H_{21}(\theta) \frac{z^2\bar{z}}{2} + \cdots \end{aligned} \quad (30)$$

Near the origin, on the manifold C_0 , we have $\dot{\mathbf{w}} = \mathbf{w}_z \dot{z} + \mathbf{w}_{\bar{z}} \dot{\bar{z}}$. Using (25) and (27) to replace $\mathbf{w}_z \dot{z}$ (and their conjugates, by their power series expansion) and equating with (29), we obtain the following operator equations:

$$(2j\omega_0 - \mathcal{A})\mathbf{w}_{20}(\theta) = H_{20}(\theta), \quad (31)$$

$$-\mathcal{A}\mathbf{w}_{11} = H_{11}(\theta), \quad (32)$$

$$-(2j\omega_0 + \mathcal{A})\mathbf{w}_{02}(\theta) = H_{02}(\theta). \quad (33)$$

We start by observing that

$$\begin{aligned} \mathbf{L}_t(\theta) &= \mathbf{w}_{20}(\theta) \frac{z^2}{2} + \mathbf{w}_{02}(\theta) \frac{\bar{z}^2}{2} + \mathbf{w}_{11}(\theta) z\bar{z} \\ &\quad + zq(\theta) + \bar{z}\bar{q}(\theta) + \cdots \end{aligned}$$

From the Hopf bifurcation analysis [1], we know that the coefficients of z^2 , \bar{z}^2 , $z^2\bar{z}$, and $z\bar{z}$ terms are used to approximate the system dynamics. Hence, we only retain these terms in the expansions. To that end, from (19), we evaluate the requisite terms. These are given by

$$\begin{aligned} v_{i,t}(-\tau_i)v_{i,t}(-\tau_i) &= (2\phi_l \phi_{i-1} e^{-j2\omega_0\tau_i}) \frac{z^2}{2} \\ &\quad + (2\bar{\phi}_l \bar{\phi}_{i-1} e^{j2\omega_0\tau_i}) \frac{\bar{z}^2}{2} + (\phi_{i-1} \bar{\phi}_l + \phi_l \bar{\phi}_{i-1}) z\bar{z} \\ &\quad + ((w_{20l}(-\tau_i) \bar{\phi}_{i-1} + w_{20i}(-\tau_i) \phi_l) e^{j\omega_0\tau_i}) \frac{z^2\bar{z}}{2} \\ &\quad + (2(w_{11l}(-\tau_i) \phi_{i-1} + w_{11i}(-\tau_i) \phi_l) e^{-j\omega_0\tau_i}) \frac{z^2\bar{z}}{2}, \end{aligned} \quad (34)$$

$$\begin{aligned} v_{l,t}(-\tau_i)v_{n,t}(-\tau_i)v_{i,t}(-\tau_i) &= (2\phi_l \phi_{i-1} \bar{\phi}_n e^{-j\omega_0\tau_i}) \frac{z^2\bar{z}}{2} \\ &\quad + (2\phi_n (\phi_l \bar{\phi}_{i-1} + \phi_{i-1} \bar{\phi}_l) e^{-j\omega_0\tau_i}) \frac{z^2\bar{z}}{2}. \end{aligned} \quad (35)$$

Substituting (34) and (35) in (19) yields the aggregation of the non-linear terms. For each $i \in \{1, 2, \dots, N\}$, it has the form:

$$\mathcal{F}_i = \mathcal{F}_{20i} \frac{z^2}{2} + \mathcal{F}_{02i} \frac{\bar{z}^2}{2} + \mathcal{F}_{11i} z\bar{z} + \mathcal{F}_{21i} \frac{z^2\bar{z}}{2}. \quad (36)$$

The expressions for the above coefficients can be derived explicitly. Due to space constraints, we omit them here.

We represent the vector of non-linearities used in (26) as $\mathcal{F}_0 = [\mathcal{F}_1 \ \mathcal{F}_2 \ \dots \ \mathcal{F}_N]^T$. Next, we compute g using \mathcal{F}_0 as

$$g(z, \bar{z}) = \bar{p}(0) \cdot \mathcal{F}_0 = \bar{B} \sum_{l=1}^N \bar{\psi}_{N-l} \mathcal{F}_l. \quad (37)$$

Substituting (36) in (37), and comparing with (28), we obtain

$$g_x = \bar{B} \sum_{l=1}^N \bar{\psi}_{N-l} \mathcal{F}_{xl}, \quad (38)$$

where $x \in \{20, 02, 11, 21\}$. Using (38), the corresponding coefficients can be computed. However, computing g_{21} requires $\mathbf{w}_{20}(\theta)$ and $\mathbf{w}_{11}(\theta)$. Hence, we perform the requisite computation next. For $\theta \in [-\tau, 0)$, H can be simplified as

$$\begin{aligned} H(z, \bar{z}, \theta) &= -\text{Real}(\bar{p}(0) \cdot \mathcal{F}_0 q(\theta)), \\ &= -\left(g_{20} \frac{z^2}{2} + g_{02} \frac{\bar{z}^2}{2} + g_{11} z\bar{z} + \dots \right) q(\theta) \\ &\quad - \left(\bar{g}_{20} \frac{\bar{z}^2}{2} + \bar{g}_{02} \frac{z^2}{2} + \bar{g}_{11} z\bar{z} + \dots \right) \bar{q}(\theta), \end{aligned}$$

which, when compared with (30), yields

$$H_{20}(\theta) = -g_{20}q(\theta) - \bar{g}_{20}\bar{q}(\theta), \quad (39)$$

$$H_{11}(\theta) = -g_{11}q(\theta) - \bar{g}_{11}\bar{q}(\theta). \quad (40)$$

From (23), (31) and (32), we obtain the following ODEs:

$$\dot{\mathbf{w}}_{20}(\theta) = 2j\omega_0 \mathbf{w}_{20}(\theta) + g_{20}q(\theta) + \bar{g}_{20}\bar{q}(\theta), \quad (41)$$

$$\dot{\mathbf{w}}_{11}(\theta) = g_{11}q(\theta) + \bar{g}_{11}\bar{q}(\theta). \quad (42)$$

Solving (41) and (42), we obtain

$$\mathbf{w}_{20}(\theta) = -\frac{g_{20}}{j\omega_0} q(0) e^{j\omega_0\theta} - \frac{\bar{g}_{20}}{3j\omega_0} \bar{q}(0) e^{-j\omega_0\theta} + \mathbf{e} e^{2j\omega_0\theta},$$

$$\mathbf{w}_{11}(\theta) = \frac{g_{11}}{j\omega_0} q(0) e^{j\omega_0\theta} - \frac{\bar{g}_{11}}{j\omega_0} \bar{q}(0) e^{-j\omega_0\theta} + \mathbf{f},$$

for some vectors \mathbf{e} and \mathbf{f} , to be determined.

To that end, we begin by defining the following vector: $\tilde{\mathcal{F}}_{20} \triangleq [\mathcal{F}_{201} \ \mathcal{F}_{202} \ \dots \ \mathcal{F}_{20N}]^T$. Equating (39) and (31), and simplifying, yields the operator equation: $2j\omega_0 \mathbf{e} - \mathcal{A}(\mathbf{e} e^{2j\omega_0\theta}) = \tilde{\mathcal{F}}_{20}$. On solving this, we obtain, for $i \in \{1, 2, \dots, N\}$,

$$\mathbf{e}_i = \frac{\mathcal{F}_{20i} + \beta_{i-1}^* e^{-j\omega_0\tau_{i-1}} \mathbf{e}_{i-1}}{2j\omega_0 + \beta_i^* e^{-j\omega_0\tau_i}},$$

where $\mathbf{e}_0 = 0$ for notational brevity.

Next, equating (40) and (32), and simplifying, we obtain the operator equation $\mathcal{A}\mathbf{f} = -\tilde{\mathcal{F}}_{11}$, with $\tilde{\mathcal{F}}_{11} \triangleq [\mathcal{F}_{111} \ \mathcal{F}_{112} \ \dots \ \mathcal{F}_{11N}]^T$. On solving, we obtain:

$$\mathbf{f}_i = \frac{\mathcal{F}_{11i} + \beta_{i-1}^* \mathbf{f}_{i-1}}{\beta_i^*},$$

for $i \in \{1, 2, \dots, N\}$, where $\mathbf{f}_0 = 0$ for notational brevity. Thus, we have obtained expressions for the vectors \mathbf{e} and \mathbf{f} required to compute $\mathbf{w}_{20}(\theta)$ and $\mathbf{w}_{11}(\theta)$. This, in turn, facilitates the computation of g_{21} . We can now compute

$$\begin{aligned} c_1(0) &= \frac{j}{2\omega_0} \left(g_{20}g_{11} - 2|g_{11}|^2 - \frac{1}{3}|g_{02}|^2 \right) + \frac{g_{21}}{2}, \\ \alpha'(0) &= \text{Real} \left(\frac{d\lambda}{d\tau_i} \right)_{\tau_i=\tau_{icr}}, \quad \mu_2 = -\frac{\text{Real}(c_1(0))}{\alpha'(0)}, \text{ and} \\ \beta_2 &= 2\text{Real}(c_1(0)). \end{aligned}$$

Here, $c_1(0)$ is known as the Lyapunov coefficient and β_2 is the Floquet exponent. These are useful since [1]

- (i) If $\mu_2 > 0$, then the bifurcation is *supercritical*, whereas if $\mu_2 < 0$, then the bifurcation is *subcritical*.
- (ii) If $\beta_2 > 0$, then the limit cycle is *asymptotically orbitally unstable*, whereas if $\beta_2 < 0$, then the limit cycle is *asymptotically orbitally stable*.

Since the derived equations are algebraically cumbersome, we present a numerical example to help derive some insights.

C. Numerical example

We use the scientific computation software MATLAB to evaluate the required quantities. Throughout, we use SI units.

We consider a platoon of 7 vehicles, *i.e.*, $N = 6$, and assume that the 5th vehicle undergoes a Hopf bifurcation. We vary m keeping the other parameters fixed to: $\dot{x}_0 = 5$, $\alpha_1 = 0.3$, $\alpha_2 = 0.5$, $\alpha_3 = 0.2$, $\alpha_4 = 0.4$, $\alpha_5 = 0.1$, $\alpha_6 = 0.6$, $\tau_1 = 1.2$, $\tau_2 = 1.7$, $\tau_3 = 2$, $\tau_4 = 2.7768$, $\tau_5 = 0.8$, $\tau_6 = 0.3$. The values of μ_2 and β_2 are as tabulated below:

SI Number	m	μ_2	β_2
1	-2	60.8590	-0.3548
2	-1.5	16.7612	-0.2185
3	-1	3.2648	-0.0952
4	1	43.4211	-31.6383
5	1.5	439.6295	-716.2806
6	2	2.4461×10^3	-8.9116×10^3

In each of these cases, $\mu_2 > 0$ and $\beta_2 < 0$. Hence, each system undergoes a *supercritical* Hopf bifurcation resulting in asymptotically orbitally *stable* limit cycles. We note from (14) that $\alpha'(0) > 0$. Hence, μ_2 and β_2 will necessarily have opposite signs. Further, extensive numerical computations hint at the absence of subcritical Hopf bifurcation in the RCCFM-DAF.

IV. NUMERICAL COMPUTATIONS

We now present a numerically constructed bifurcation diagram that complements our analysis, obtained using MATLAB. We obtain the bifurcation diagram by solving system (6) using the ‘method of steps’ [13, Chapter 5], and plotting the maximum and the minimum values pertaining to the envelope of the steady-state solution.

We let $N = 4$, and assume that the 3rd vehicle undergoes a Hopf bifurcation. We fix the parameter values to: $\alpha_1 = 0.1$, $\alpha_2 = 0.5$, $\alpha_3 = 0.3$, $\tau_1 = 0.6$, $\tau_2 = 1$, $\tau_3 = 0.2$, $m = 1.5$. We then compute \dot{x}_0 such that $\tau_{2cr} = 1$, for

ACKNOWLEDGEMENTS

This work is undertaken as a part of an Information Technology Research Academy (ITRA), Media Lab Asia, project titled “De-congesting India’s transportation networks.” The authors are also thankful to Debayani Ghosh and Sreelakshmi Manjunath for many helpful discussions, and the reviewers for their helpful comments.

REFERENCES

- [1] B.D. Hassard, N.D. Kazarinoff and Y.-H. Wan, “Theory and Applications of Hopf Bifurcation.”, *Cambridge University Press*, 1981.
- [2] D. Chowdhury, L. Santen and A. Schadschneider, “Statistical physics of vehicular traffic and some related systems”, *Physical Reports*, vol. 329, pp. 199-329, 2000.
- [3] D.C. Gazis, R. Herman and R.W. Rothery, “Nonlinear follow-the-leader models of traffic flow”, *Operations Research*, vol. 9, pp. 545-567, 1961.
- [4] D. Helbing, “Traffic and related self-driven many-particle systems”, *Reviews of Modern Physics*, vol. 73, pp. 1067-1141, 2001.
- [5] E.A. Unwin and L. Duckstein, “Stability of reciprocal-spacing type car-following models”, *Transportation Science*, vol. 1, pp. 95-108, 1967.
- [6] G.K. Kamath, K. Jagannathan and G. Raina, “Car-following models with delayed feedback: local stability and Hopf bifurcation”, in *Proceedings of the 53rd Annual Allerton Conference on Communication, Control and Computing*, 2015.
- [7] G. Orosz and G. Stépán, “Subcritical Hopf bifurcations in a car-following model with reaction-time delay”, *Proceedings of the Royal Society A*, vol. 642, pp. 2643-2670, 2006.
- [8] H. Gomi and M. Kawato, “Neural network control for a closed-loop system using feedback-error-learning”, *Neural Networks*, vol. 6, pp. 933946, 1993.
- [9] I. Györi and G. Ladas, “Oscillation Theory of Delay Differential Equations With Applications”, *Clarendon Press*, 1991.
- [10] J.I. Ge and G. Orosz, “Dynamics of connected vehicle systems with delayed acceleration feedback”, *Transportation Research Part C*, vol. 46, pp. 46-64, 2014.
- [11] J.K. Hale and S.M.V. Lunel, “Introduction to Functional Differential Equations”, *Springer-Verlag*, 2011.
- [12] M. Bando, K. Hasebe, K. Nakanishi and A. Nakayama, “Analysis of optimal velocity model with explicit delay”, *Physical Review E*, vol. 58, pp. 5429-5435, 1998.
- [13] R.D. Driver, “Ordinary and Delay Differential Equations”, *Springer-Verlag*, 1977.
- [14] R.E. Chandler, R. Herman and E.W. Montroll, “Traffic dynamics: studies in car following”, *Operations Research*, vol. 6, pp. 165-184, 1958.
- [15] R.E. Wilson and J.A. Ward, “Car-following models: fifty years of linear stability analysis - a mathematical perspective”, *Transportation Planning and Technology*, vol. 34, pp. 3-18, 2011.
- [16] R. Herman, E.W. Montroll, R.B. Potts and R.W. Rothery, “Traffic dynamics: analysis of stability in car following”, *Operations Research*, vol. 7, pp. 86-106, 1959.
- [17] R. Olfati-Saber and R.M. Murray, “Consensus problems in networks of agents with switching topology and time-delays”, *IEEE Transactions on Automatic Control*, vol. 49, 2004.
- [18] R. Sipahi and S.I. Niculescu, “Analytical stability study of a deterministic car following model under multiple delay interactions”, in *Proceedings of Mechanical and Industrial Engineering Faculty Publications*, 2006.
- [19] T. Insperger, J. Milton and G. Stépán, “Acceleration feedback improves balancing against reflex delay”, *Journal of the Royal Society Interface*, Vol. 10, pp. 1-12, 2013.
- [20] T. Vyhliđal, N. Olgac and V. Kučera, “Delayed resonator with acceleration feedback – Complete stability analysis by spectral methods and vibration absorber design”, *Journal of Sound and Vibration*, vol. 333, pp. 6781-6795, 2014.
- [21] X. Zhang and D.F. Jarrett, “Stability analysis of the classical car-following model”, *Transportation Research Part B*, vol. 31, pp. 441-462, 1997.
- [22] W. Rudin, “Real & Complex Analysis”, *Tata McGraw Hill Publications*, Third Edition, 1987.

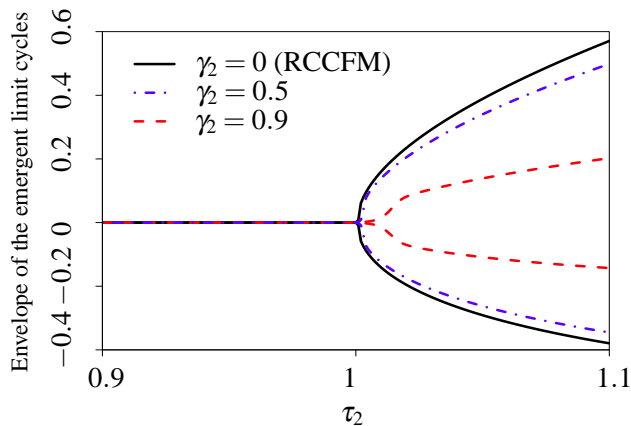


Fig. 2. *Bifurcation diagram*: Plot of variation in the envelope of the emergent limit cycles with respect to τ_2 , for $\gamma_2 \in \{0, 0.5, 0.9\}$.

simplicity. We then vary γ_2 to study the effect of DAF on the amplitude of the emergent limit cycles. As seen in Fig. 2, an increase in the DAF signal strength reduces the amplitude of the emergent limit cycles. Further, note the effect of the system non-linearity: The change in amplitude is larger when γ_2 is increased from 0.5 to 0.9, as opposed to when it is varied from 0 (*i.e.*, RCCFM) to 0.5.

V. CONCLUDING REMARKS

A. Conclusions

In this paper, we highlighted the effects of DAF on the qualitative dynamical properties of a platoon of self-driven vehicles traversing a straight road. We proved that the RCCFM-DAF undergoes a Hopf bifurcation, which implies that DAF preserves the mechanics by which the RCCFM loses stability. The resulting necessary and sufficient condition for local stability and the frequency of the emergent limit cycles characterised the effects of DAF on the RCCFM: (i) The stable region shrinks, and (ii) the said frequency increases, with an increase in the DAF signal strength.

We then characterised the type of Hopf bifurcation and the asymptotic orbital stability of the emergent limit cycles for the RCCFM. An appropriately chosen linear transformation then allowed us to obtain insights into the RCCFM-DAF. Our analysis was complemented by a stability chart and a numerically constructed bifurcation diagram. The bifurcation diagram revealed the decrease in the envelope of the emergent limit cycles, as a consequence of incorporating DAF. Thus, our work revealed two ways in which DAF was detrimental to the RCCFM; namely, decreasing the robustness to the reaction delay, and possibly leading to jerky vehicular motion and degradation of ride quality.

B. Avenues for further research

There are numerous avenues that merit further investigation. As an extension of this work, the effect of DAF on the rate of convergence and the region of non-oscillatory convergence remains to be investigated.